Biochimica et Biophysica Acta 1804 (2010) 2177–2182

Contents lists available at ScienceDirect

Biochimica et Biophysica Acta

journal homepage: www.elsevier.com/locate/bbapap

Structural analysis and molecular modeling of the RvH2-e functional unit of *Rapana venosa* hemocyanin

Ludmila Velkova [a], Pavlina Dolashka [a,*], Aleksander Dolashki [b], Wolfgang Voelter [b], Boris Atanasov [a,*]

[a] Institute of Organic Chemistry, Bulgarian Academy of Sciences, G. Bonchev 9, Sofia 1113, Bulgaria
[b] Interfacultary Institute of Biochemistry, University of Tübingen, Hoppe-Seyler-Strasse 4, D-72076 Tübingen, Germany

ARTICLE INFO

Article history:
Received 29 April 2010
Received in revised form 20 August 2010
Accepted 23 August 2010
Available online 31 August 2010

Keywords:
Rapana venosa hemocyanin
Functional unit RvH2-e
Circular dichroism spectra
Reversible denaturation
Thermodinamic characteristics
Protein 3D- structure

ABSTRACT

Rapana venosa hemocyanin (RvH), a circulating glycoprotein of the marine snail, has a complex structure. To provide details on the stability of the protein, one functional unit, RvH2-e, was compared with the native molecule and the structural subunits, RvH1 and RvH2, via pH–*T* diagrams, typical phase portraits for stability and denaturation reversibility. By analyzing the *T* transition curves of RvH2-e at different pH values, several parameters of the thermodynamic functions were obtained. Increasing the temperature from 25 °C to 55 °C, the reversibility of the molecule of protein also increases, opening a reversibility window within the range of pH 4.0–8.0. On analyzing the pH transition curves, the start of the acid denaturation (below pH 6) and alkaline denaturation (above pH 9) was determined to be between 20 °C and 35 °C. For this range, the thermodynamic functions $\Delta H°$ and $\Delta G°$ for a standard temperature of 25 °C were calculated.

1. Introduction

Hemocyanins (HCs) are giant oxygen transport proteins found in the hemolymph of many arthropods and mollusks [1–4]. The native molecules of molluskan HCs contain 1, 2 or 3 different isoforms, aggregated to decamers and didecamers [5]. The largest HC quaternary structures are found as single decamers in cephalopods and chitons, such as *Octopus dofleini* (OdH) [6], *Nautilus pompilius* (NpH) [7], *Sepia officinalis* [8] and *Loligo pealei* [9]. Two distinct native decameric forms were isolated in gastropods from *Megathura crenulata* (KLH) [10], *Haliotis tuberculata* (HtH) [11,12], *Aplycia californica* (ApH) [13], *Concholepas concholepas* (CcH) [14] and *Rapana venosa* (RvH) [15,16]. Although molluskan HCs are similar in their quaternary structure, all structural subunits are composed of 7 or 8 functional units (FU) [6–16]. The two structurally and functionally distinct HC isoforms of gastropodan HCs KLH, HtH and RvH, with a mass of about 400 kDa are folded into 8 linked globular FUs, termed FU-a to FU-h (from the N- to the C-terminus). Each FU of about 50 kDa contains two copper atoms that can reversibly bind one dioxygen molecule [10–12].

The structure and properties of molluskan and arthropodan HCs have been studied using different methods and techniques; e.g. the temperature, pH and guanidinium chloride-induced unfolding of arthropodan HCs from *Carcinus aestuarii* [17,18], *Lymulus poliphemus* [19], Chinese mitten crab (*Eriocheir japonica sinensis*) [20] have been very well studied by UV-vis, fluorescence, synchronous fluorescence, and circular dichroism (CD).

Molluskan HCs are immunologically active proteins. Recently, it has been reported that *R. venosa* and *Helix vulgaris* HCs display antitumor and antiparasitic activities [21–24]. Therefore, studies on the properties and stability of these proteins are of broader interest. Although the structure and function of molluskan HCs have been investigated in depth, only a few studies have addressed the stability of dioxygen carriers [25–29]. We report for the first time on the stability (pH and thermostability) of a molluskan HC [30] from the marine gastropod *R. venosa*, using spectroscopic methods.

Rapana thomasiana (renamed as *R. venosa*) HC was investigated by differential scanning calorimetry [31]. Although the authors reported that the thermal denaturation of *R. thomasiana* HCs is irreversible, several parameters of reversibility thermodynamics such as calorimetric enthalpy ΔH_{cal} were measured [31]. However, because of the irreversibility of thermal denaturation of these large complexes, thermodynamic parameters cannot be obtained. It is possible to obtain the kinetic information only indirectly at non-fixed parameterization.

Therefore, in the present study, new large sets of pH–*T* data characterizing the conformational stability of one functional unit of *R. venosa* HC were compared with those of the structural subunits and the whole RvH protein.

* Corresponding authors. P. Dolashka is to be contacted at Institute of Organic Chemistry with Centre of Phytochemistry, Bulgarian Academy of Sciences, 9 G. Bonchev Street, 1113 Sofia, Bulgaria. Tel.: +359 29606163; fax: +359 28700225. B. Atanasov, Tel.: +359 29606123; fax: +359 28700225.
E-mail addresses: pda54@abv.bg (P. Dolashka), boris@orgchm.bas.bg (B. Atanasov).

1570-9639/$ – see front matter © 2010 Elsevier B.V. All rights reserved.
doi:10.1016/j.bbapap.2010.08.009

2. Materials and methods

2.1. Isolation of the RvH2-e FU

R. venosa HC (RvH) and its 2 structural subunits RvH1 and RvH2 were isolated from the hemolymph of marine snails living in the Black Sea as described previously [5]. After treatment of the RvH2 structural subunit with trypsin in a ratio of 400:1 and incubation at 37 °C for 4 h, FU RvH2-e was isolated on an ion-exchange Resource Q 6 ml (Pharmacia) column using a fast protein liquid chromatography system by elution with 50 mM Tris–HCl buffer (pH 8.2) using a 0.0–0.5 M NaCl gradient as described previously [15]. The main molecular characteristics of RvH2-e are: MW = 47835.1 Da, absorbance coefficient $\varepsilon = 93{,}000\ M^{-1}\ cm^{-1}$ at 278 nm, pH 7.5 and 20 °C [32]. This protein has 2 absorption bands at 280 nm and at 347 nm. The ratio of purity (R_z) used for protein concentration determination in solution was $R_z = A_{347}/A_{280} = 0.210$.

2.2. CD measurements

CD spectra were recorded on a J-720 dichrograph (Jasco, Tokyo, Japan). Cylindrical temperature-controlled quartz cells with a path length of 10 mm were used in all experiments. CD spectra were recorded in the range between 200 and 250 nm with a bandwidth of 1 nm, a scan speed of 50 nm/min, and a time constant of 8.0 s. The cocktail buffer at ionic strength 0.075 (with constant salt concentration of 20 mM for each component) was adjusted to the given pH in the range pH 2–12.

Protein solutions were prepared in 20 mM cocktail buffer (20 mM sodium phosphate buffer, pH 7.4–5.8, 20 mM sodium acetate buffer, pH 5.4–3.6, and 20 mM glycine–HCl buffer, 3.4–1.2 in equal volumes). The final mixtures with protein concentrations of 20 μM were incubated for 20 min at room temperature before optical measurements. Each spectrum was the average of four scans. The results were expressed as mean residue ellipticity (MRE, $[\Theta]_{222}$) in deg cm^2 $dmol^{-1}$.

The temperatures were thermostatically controlled using a NESLAB thermostat model RTE-110, connected to a digital programming controller, and a thermocouple placed inside the optical cell. Two approaches were applied for evaluation of effective thermodynamic functions and determination of cross-overlapped CD data:

(1) pH-dependent thermal denaturation. For thermal denaturation, the CD spectrum of each protein solution sample in cocktail buffer at different pH values (from 1.5 to 12.0) was measured after 20 min incubation at temperatures from 20 °C to 85 °C. The $[\theta]_{222}$ values were recorded in intervals of 5.0 ± 0.2 °C.
(2) *T*-dependent pH denaturation. For pH-dependent CD, the spectra of each sample of standardized HC solution (see first approach) were recorded in 5 °C steps at different temperatures from 20 to 85 °C over a wide range of pH values (2–12), with increments of ~0.5 after incubation for 20 min. The extreme values at 222 nm were digitalized and recalculated in $[\theta]_{222}$ units (deg cm^2/dmol).

Two independent sets of experimental data: (a) $[\theta]_{222}$ as a function of *T* °C for 14–15 samples at different pH and (b) $[\theta]_{222}$ as a function of pH for 14–15 samples at different *T* °C, were collected. The experimental matrix $[\theta]_{exp}(T)$ was converted to the calculated $[\theta]_{cal}$(pH) matrix using data in *T* dissections at different pH values, and the matrix $[\theta]_{exp}$(pH) was converted to $[\theta]_{cal}(T)$ using data in pH dissections at different temperatures. The total reversibility of the system suggests independence of the final states from the path(s) of their realization. Thus, if our system is reversible, then $[\theta]_{cal}(T)$ curves will be identical to the $[\theta]_{exp}(T)$ curves and the $[\theta]_{cal}$(pH) curves will be identical to the $[\theta]_{exp}$(pH) curves. To prove this strong requirement of reversibility, we extracted each pair of curves with the same (*T*, pH) signatures and plotted these as $\Delta[\theta](T)$ and $\Delta[\theta]$(pH) [30,33]. The relative percentage of $\Delta[\theta]$ with steps of 4% was used to construct *T*–pH phase diagrams of RvH2-e within 80–100% reversibility.

2.3. Estimation of the effective melting temperatures (T_m) and the T–pH phase diagram

From averaged $[\theta]_{exp}(T)$ curves, neglecting the complexity of the averaged curve and an oversimplified assumption for the two-state mechanism (N↔D) (crude zero approximation), the melting temperature T_m was estimated [34] as the temperature of half-denaturation for RvH2-e:

$$\Delta H_{eff} = 4R(273 + T\,^{\circ}C)_m^2 / 1000 \times \Delta T(\text{kcal / mol})$$

The initial or native state (N) and the final or denatured state (D) were analyzed. Several plots were taken within the interval of pH 5–9 (region of high reversibility). All curves were symmetrical with a well-defined inflex point of T_m. This was improved after linearization of the curves in van't Hoff's coordinates $\ln K_{obs}/R$ vs. $1/T$. The slopes of these lines give the effective enthalpies (van't Hoff's) ΔH_{vH}.

With knowledge of T_m(pH), ΔH_{vH}(pH) and the heat capacity ΔC_p the pH-dependent thermodynamic stability of the protein could be obtained as follows: T_m was used as an integral characteristic of a structure with the expectation that there will be *T*-/pH-dependent changes in quaternary structure [35]. The van't Hoff's analysis of these data was made using plots of $\log K_{obs}/R$ vs. $1/T$ and calculating $\Delta G_{vh} = -RT\ln K_{obs} = -RT[Y/(1-Y)]$, where *Y* is the relative ($0<Y<1$) change of $[\theta]_{exp}$ as a function of temperature (in K). To compare all data under standard conditions ($T_o = 298$ K and $\Delta C_p = \partial \Delta H_{m,i}/\partial T_{m,i}$), ΔG^o_{vh} was calculated using [34]:

$$\Delta H_i^o = \Delta H_{m,i} - \Delta C_p\left(T_{m,i} - T_o\right)\ (\text{kcal / mol})$$

$$\Delta S_i^o = \Delta H_{m,i} / T_{m,i} - \Delta C_p \ln\left(T_{m,i} / T_o\right)\ (\text{cal / (molGrad)})$$

$$\Delta G^o_{vh,i} = \Delta H_{m,i}\left[1 - \left(T_o / T_{m,i}\right)\right] - \Delta C_p\left[\left(T_{m,i} - T_o\right) - T\ln\left(T_o / T_{m,i}\right)\right]\ (\text{kcal / mol})$$

3. Results and discussion

In the literature, there are a limited number of papers on the biophysical and structural properties of the function and stability of molluskan HC. The conformational stability of the native didecameric aggregates of RvH [26] and their isolated structural subunits towards various denaturants (pH and guanidine hydrochloride (Gdn·HCl)) indicate that hydrophilic and polar forces, whereby both the oxy- and apo-forms of the protein are considered, stabilize the quaternary structure [26]. Denaturation studies of HCs by Gdn·HCl indicate that the denaturation process consists of 2 steps: dissociation of the native molecule into its structural subunits and denaturation of the subunits at concentrations of Gdn·HCl > 1.5 M [26]. In addition, 2 denaturation steps are observed after keeping the protein in buffer solutions at different pH values, with different pH stabilities for the holo-oxy and apo-HC forms [26]. However, such studies may be complicated by the fact that it may be difficult to distinguish between the effects on the quaternary structure of the oligomeric protein (initial dissociation) and those on the tertiary and secondary structure (i.e. subunit unfolding), depending on the dissociation conditions. There is evidence of different re-association behaviors of the purified (dissociated) structural subunits, RvH1 and RvH2, compared with the mixed subunits produced from the native molecules. Thus, neither real thermodynamic data nor structurally related activation

parameters could be obtained [30]. This limited background was the reason for the detailed physicochemical analysis presented in this report. As the thermal denaturation of the native molecule and the 2 isoforms of RvH is an irreversible process [30], under kinetic control, a successive annealing procedure was applied to analyze the behavior and stability of one functional unit, RvH2-e.

3.1. Thermal stability of RvH2-e in buffers with different pH

To determine the thermal stability of RvH2-e, the *T* transition curves at different pHs were analyzed. CD spectra of RvH2-e, in cocktail buffers, were measured in the region from 200 to 250 nm and the temperature was continuously varied from 20 to 95 °C at a constant rate by carefully adjusting the heating control of the water bath. The CD spectrum for the native FU (pH 8.0) has 2 minima, one at 208 nm and the other at 222 nm, which is a characteristic feature of α-helical protein (data are not shown). The intermediate state relative to the native state was determined by ellipticity changes at 222 nm as a function of temperature. As shown in Fig. 1, the initial feature of the *T* transition curves is the presence of *T*-induced changes within a wide temperature interval (20–85 °C). A characteristic of reversible protein denaturation is the assumption of common end states of relatively similar disordered structures. The amplitude $\Delta[\theta]_N - \Delta[\theta]_D$ for curves at different pHs is slightly decreased for extreme pH values. The relatively small changes of the initial $[\theta]_{222}$ at high temperatures indicate that the main part of the structural elements are preserved, especially at neutral pH and at high temperatures. Thus, complete *T*-dependent unfolding was not detected and probably even at temperatures above 85 °C the structure is not a random coil, i.e. the proteins retain their globular state (Fig. 1). However, the curves obtained for the native RvH and its 2 subunits, RvH1 and RvH2, clearly show that they are composed of 2 or more components and represent complex temperature transitions [30]. This is not surprising because of the complexity of the structure of gastropod HC, created from multiple subunits each containing seven or eight similar, but not identical, FUs.

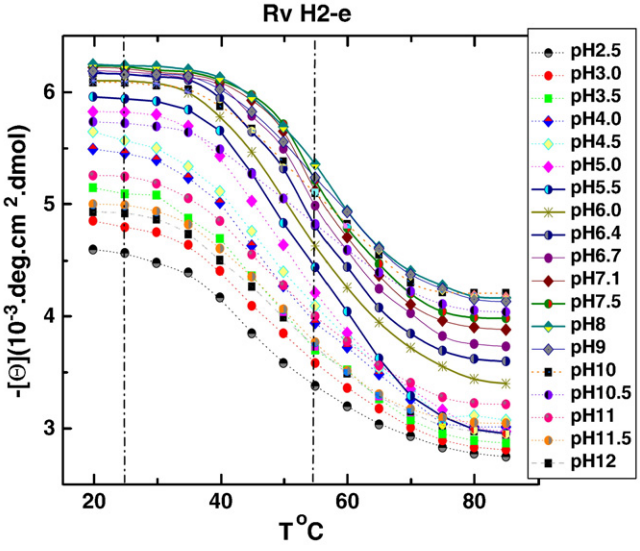

Fig. 1. Thermal unfolding experiments of RvH2-e at exactly the same protein concentrations and buffer contents measured by circular dichroism spectra at 222 mn. The *T*-induced changes are obtained over a wide temperature interval (20–85 °C) at fixed pH (2.5–12). Curves considered to be reversible (solid lines) are shown within the two vertical dashed lines. All other conditions are irreversible.

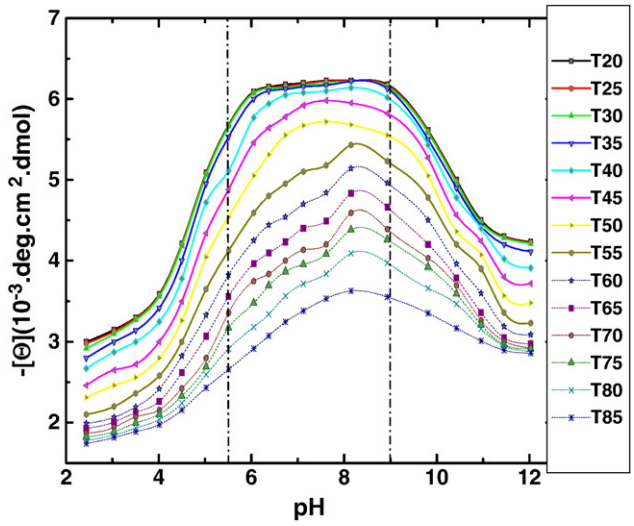

Fig. 2. Influence of pH on $[\theta]_{222}$ of RvH2-e at different temperatures. Part of the curves considered to be reversible (in solid) is locked in vertical dashed lines. All others curves are assumed as irreversible.

3.2. Influence of pH on the stability of RvH2-e at different temperatures

Changes in the secondary structure of FU RvH2-e at different temperatures (25–90 °C) as a function of pH (pH 2–12) were followed by near UV-CD measurements in the region between 200 and 250 nm. The $[\theta]_{222}$ vs. pH plots, shown in Fig. 2, represent a set of smooth and partially bell-shaped curves with maxima between pH 5 and 9 and non-symmetric acidic and alkaline extremes, but without any obvious sigmoid feature at extreme pH. In contrast, the native molecule of RvH and both isoforms revealed different behavior for the complete set of pH curves at different temperatures, suggesting a number of pH-dependent processes, as reported in our previous work [30]. In the alkaline part (pH 8–12), relative changes are too small and non-cooperative (within a wide pH interval), indicating that alkaline denaturation cannot be achieved as a reversible process [30].

The temperature-induced unfolding of KLH at pH 7.4, 2.8 and 1.2 was measured by MRE at 222 nm and induced unfolding transitions of 2 (native (N) and molten globule (N*)) states, which are cooperative and non-cooperative processes, respectively [29]. Temperature-induced non-cooperative unfolding of KLH at pH 2.8 indicated continuous loss in the secondary structure content in the temperature range 20–80 °C. These results obtained from KLH [29] and RvH [30]

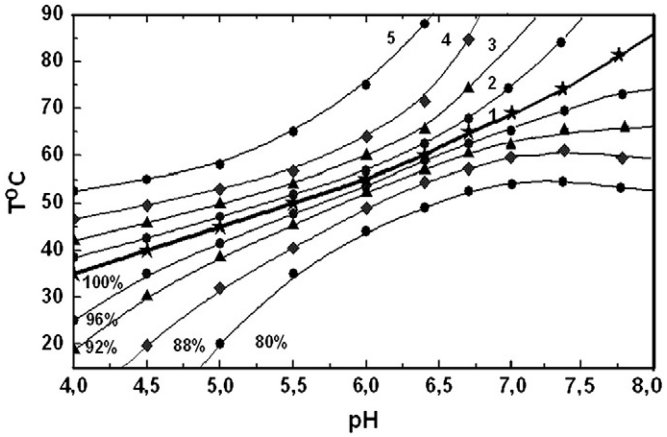

Fig. 3. Iso-lines (contours) at equal renaturation reversibility of RvH2-e. The surface between *T*–pH lines corresponds to reversibility (in %) as follows: 100 (1), 96 (2), 92 (3), 88 (4) and lower then 80 (5).

show that the unfolding of a molten globule state is a non-cooperative process.

Both pH-acid and pH-alkaline denaturation are poorly presented in all curves at extreme pH regions. The data sets of RvH2-e can be accounted for by an increased stability due to self-association and formation of a quaternary structure. The $[\theta]_{222}$/pH values within a pH range of 6.5–8.5 have a wide plateau at low temperatures (20–40 °C) and curves that are independent of pH. Thus, no titrable groups of RvH2-e were observed in this pH region, which is the main reason for structural stability. The same conclusion is also valid for KLH. Comparing the 2 sets of RvH2-e curves $[\theta]_{222}$(pH) at low and high pH values and at low temperatures (25–45 °C), both are less pH dependent than at higher temperatures (50 °C and above). However, in the case of the structural subunits, RvH1 and RvH2, in the native state and in the pH range (6.5–9.0), the presence of a slight peak was observed, indicating the presence of 2 ionization processes (due to carboxylates and imidazoles), with an opposing influence on the left (L, acidic) and right (R, alkaline) limbs of $[\theta]_{222}$(pH) [30].

Table 1
The main thermodynamic functions of reversible RvH2-e denaturation.

RvH2-e function unit				
pH	T_m	ΔH_m	ΔH_o	ΔG^o_{exp}
5.5	324.7	6.68	−8.0	−28.20
6.0	326.5	7.65	−8.0	−29.98
6.4	328.0	8.39	−8.1	−31.46
6.7	328.6	8.74	−8.0	−31.99
7.1	329.5	9.38	−8.0	−32.90
7.5	330.0	9.40	−8.1	−33.41
8.0	329.8	9.40	−7.9	−33.19

3.3. T–pH reversibility phase diagram

The traditional approach to verify the accumulation of an intermediate state during protein unfolding or refolding is to compare the unfolding curves determined under different conditions sensitive to the different structural levels of a protein molecule. A phase diagram, plotted as a *T*–pH grid of $[\theta]_{222}$, represents the pH-induced conformational changes of RvH2-e (Fig. 3). Because of the large set of experimental points in the diagram, the dissections at a given temperature for discrete pH values and vice versa (at a given pH for corresponding temperatures) were recorded and the data were converted to a new pair of data sets. If the principle of thermodynamic independence of the denaturation state from the method of achievement is correct, then one should obtain the same results. We accept that extension of the relative identity (as % of MRE) is a measure and criterion of reversibility [30]. The results from this morphing for RvH2-e are represented as lines that connect the *T*–pH points with equal reversibility (%) as 100 (1), 96 (2), 92 (3), 88 (4) and 80 (Fig. 3). We propose that this phase portrait for reversibility is valid in pH–*T* perturbations for RvH2-e, and as shown, the pH system is reversible at 25 °C. Increasing the temperature within the range 30–55 °C, the reversibility increases and opens a window within the range of pH of 4.0–8.0.

Different behavior was observed in phase portraits for the native molecule and 2 structural subunits of RvH. In the case of RvH, thermal- and pH-induced denaturation could be accompanied by dissociation into subunits because RvH is an oligomeric protein [30]. Thus, 100–80% reversibility is possible only in an acidic pH range. The multimeric intact RvH structure has a small interval of partial reversibility close to pH 4 and strong perturbance in the region of pH 7. The subunits RvH1

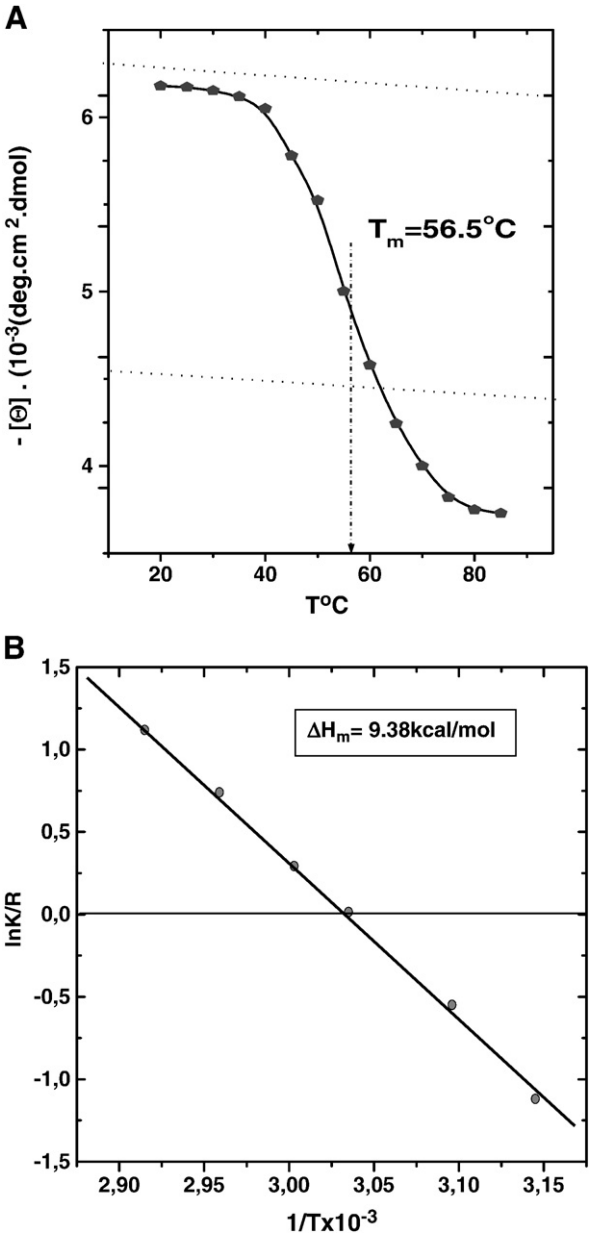

Fig. 4. (A) Plot of thermal unfolding of RvH2-e in 20 mM Tris buffer, pH 7.1. (B) Linearization of the curve in van't Hoff's coordinates $\ln K_{obs}/R$ vs $1/T$. The slope of this line gives the effective enthalpy (van't Hoff's) ΔH_{vH}.

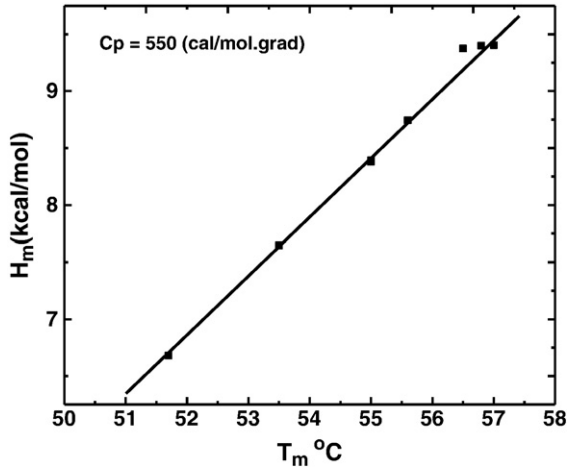

Fig. 5. Indirect determination of specific heat capacity (Cp) from ΔH_m vs. T_m within the range of pH 5.5–9.0 of the denaturation process for all pH-s.

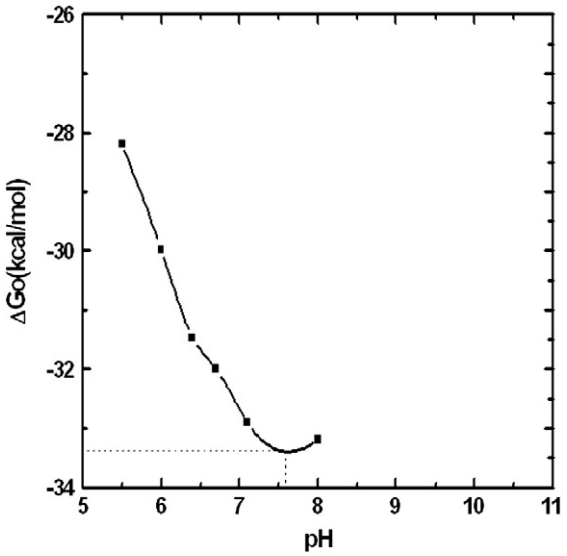

Fig. 6. The Gibbs free energy of denaturation at wide pH interval (pH-dependent stability, ΔG°_{exp}) is calculated with extrapolation to $T = 298$ K. Structural stability of reversible denaturation of RvH2-e is pH-dependent [ΔG°_{exp}(pH)].

and RvH2 show higher reversibility at 25 °C within pH intervals of 4.1–4.7 and 4.2–5.3, respectively [30].

3.4. Thermodynamic characteristics of T–pH denaturation of RvH2-e

Determination of reversibility for RvH2-e allowed several thermodynamic parameters to be calculated. For the region of high reversibility range (pH 4.0-8.0), several plots were analyzed within the pH range of 5.5–9.0, and the inflex point of T_m was determined (Fig. 4A). The effective enthalpies (van't Hoff) ΔH_{vH} were determined from the slopes of the curves $\ln K_{obs}/R$ vs. $1/T$. As shown in Fig. 4B, based on the curve at pH 7.1, a ΔH_m of 9.38 kcal/mol was calculated. Representative data for other curves are shown in Table 1.

The resulting ΔH_{vH} values are plotted as ΔH_{vH}(pH) within the pH range of 5.5–9.0. Full reversibility is demonstrated by the fact that all experimental determinations of ΔH_m within the pH range of 5.5–9.0 are located on a straight line, which gives the effective thermal capacity at fixed pressure ($\Delta C_p \approx \partial \Delta H_{vH}/\partial T$). The average *value* for ΔC_p was 550 cal/(mol grad), which is a relatively high value for proteins (Fig. 5). However, such a high value of ΔC_p is in agreement with the opening of a hydrophobic protein interior at denaturation. Both ΔH°_{exp} and ΔG°_{exp} (in kcal/mol) are recalculated for the standard temperature 298 K within the interval 5.5–9.0.

The pH-dependent part of the structural stability (ΔG°_{exp}) of reversible denaturation of RvH2-e [ΔG°_{exp}(pH)] has the shape of a normal pH-dependent stability curve. As shown in Fig. 6, the curve is pH dependent with a complex shape and has a minimum at pH 7.6. The total stability was determined experimentally to be 33.4 kcal/mol. After recalculation of ΔH° from ΔH_m for each fixed pH value at standard temperature (298 K) and within the pH range of 5.5–9.0 (determined region), it was found that ΔH° is independent of pH with a value of 8.0 kcal/mol. Based on their pH independence, these processes can be described as hydrophobic rearrangement of the quaternary structure.

Several functional units of molluskan HCs with a molecular mass of approximately 50 kDa, but different structure, have been partially studied [26–29]. They differ considerably in their carbohydrate content (0–18 wt.%). Using CD and fluorescence spectroscopy, the thermostability of the non-glycosylated FU KLH2-c, isolated from the structural subunit KLH2 of keyhole limpet *Megathura crenulata* HC, was compared with the glycosylated FU RvH1-a of *R. venosa* HC [29]. The melting temperature T_m (45 °C) and the critical temperature T_c (46 °C) were found to be less for KLH2-c compared with the glycosylated forms, which could be explained by the presence of oligosaccharide side chains and aggregation effects [29]. It was also found that most of the glycosylated functional units of *Helix pomatia* β-HC are exceptionally stable with a melting temperature in the range from 64 °C to 83 °C [28]. Although the most glycosylated functional unit (HpH-g) has the highest temperature stability, there is no linear correlation between the degree of glycosylation of the functional units and the unfolding temperature [28]. Therefore their behavior could be attributed to variations in glycan attachment sites as well as in the secondary structure. Moreover, it is known that disulfide bonds may play an important role in the conformational stability of the proteins. Generally, FUs contain 3 disulfide bridges: 2 in the mainly alpha-helical N-terminal domain and one in the C-terminal beta-sheet domain. Comparison of the sequences of two FUs of *Helix pomatia* HC suggests that the less stable functional units, HpH-b and HpH-c, lack the disulfide bond in the C-terminal domain [28].

4. Conclusion

The stability of native HC and its subunits, shown by coupled T and pH transitions (acid and alkaline denaturation), was explained by the formation of quaternary structures, which introduces additional factors, namely non-ionic forces (intra-subunit, hydrophobic and hydrogen-bonded networks of carbohydrate moiety interactions). Apparently, thermal denaturation of the native molecule and its 2 isoforms are irreversible processes and their real thermodynamic data cannot be obtained.

For the first time, we report the conditions in which reversible denaturation of the single functional unit RvH2-e can exist. The narrow range over which the system is reversible has been determined using the strongest test of 2 important thermodynamic independent variables (T and pH) in a stability phase diagram, as a result of which the real thermodynamic parameters (ΔC_p, ΔH°_{exp}, and ΔG°_{exp}) for one HC moiety were determined.

Nevertheless, the parameters obtained could not be explained by the known 3D structure of RtH2-e, because 13 residues are missing in the present x-ray structure (1LNL.pdb) and most of them are important in pH-dependent stability.

Acknowledgments

This work was supported by a research grant by the Bulgarian National Science Fund TK01-496/2009, HTC01-187 (Ukraine) and UV-L-301, DAAD -17/2007 and DFG-01/2008 (Germany). We thank to Ing. H. Stoyanov, Director of "Delta Industry" AD, Sozopol, for providing the Rapana snails.

References

[1] K.E. Van Holde, K.I. Miller, H. Decker, Hemocyanins and invertebrate evolution, J. Biol. Chem. 276 (2001) 15563–15566.
[2] H. Decker, N. Hellmann, E. Jaenicke, B. Lieb, U. Meissner, J. Markl, Minireview: recent progress in hemocyanin research, Integr. Comp. Biol. 47 (2007) 631–644.
[3] P. Dolashka-Angelova, A. Dolashki, S. Savvides, R. Hristova, J. Van Beeumen, W. Voelter, B. Devreese, U. Weser, P. Di Muro, B. Salvato, S. Stevanovic, Structure of hemocyanin subunit CaeSS2 of the Crustacean Mediterranean crab *Carcinus aestuarii*, J. Biochem. 138 (2005) 303–312.
[4] B. Lieb, B. Altenhein, J. Markl, A. Vincent, E. Olden, K. van Holde, Structures of two molluscan hemocyanin genes: significance for gene evolution, Proc. Natl Acad. Sci. USA 98 (2001) 4546–4551.
[5] P. Dolashka-Angelova, H. Schwarz, A. Dolashki, M. Beltramini, B. Salvato, M. Schick, M. Saeed, W. Voelter, Oligomeric stability of *Rapana venosa* hemocyanin (RvH) and its structural subunits, Biochim. Biophys. Acta 1646 (1–2) (2003) 77–85.
[6] K.I. Miller, M.E. Cuff, W.F. Lang, P. Varga-Weisz, K.G. Field, K.E. van Holde, Sequence of the *Octopus dofleini* hemocyanin subunit: structural and evolutionary implications, J. Mol. Biol. 278 (1998) 827–842.
[7] S. Bergmann, J. Markl, B. Lieb, The hemocyanin from a living fossil, the cephalopod *Nautilus popilius*: protein structure, den organization, and evolution, J. Mol. Evol. 62 (2006) 362–374.

[8] J. Lamy, V. You, J.-C. Taveau, N. Boisset, J.N. Lamy, Intramolecular localization of the functional units of *Sepia officinalis* hemocyanin by immunoelectron microscopy, J. Mol. Biol. 284 (1998) 1051–1074.
[9] D. Chignell, K.E. van Holde, K.I. Miller, The hemocyanin of the squid *Sepioteuthis lessoniana*: structural comparison with other cephalopod hemocyanins, Comp. Biochem. Physiol. 116B (1997) 895–902.
[10] W. Gebauer, J.R. Harris, H. Heid, M. Süling, R. Hillenbrand, S. Söhngen, A. Wegener-Strake, J. Markl, Quaternary structure, subunits and domain patterns of two discrete forms of keyhole limpet hemocyanin: KLH1 and KLH2, Zoology 98 (1994) 51–68.
[11] K. Streit, D. Jackson, B.M. Degnan, B. Lieb, Developmental expression of two *Haliotis asinina* hemocyanin isoforms, Differentiation 73 (2005) 341–349.
[12] U. Meissner, P. Dube, J. Harris, H. Stark, J. Markl, Structure of a molluscan hemocyanin didecamer (HtH1 from *Haliotis tuberculata*) at 12 Å resolution by cryoelectron microscopy, J. Mol. Biol. 298 (2000) 21–34.
[13] B. Lieb, V. Boisguerin, W. Gebauer, J. Markl, cDNA sequence, protein structure, and evolution of the single hemocyanin from *Aplysia californica*, an opisthobranch gastropod, J. Mol. Evol. 59 (2004) 1–10.
[14] P. De Ioannes, B. Moltedo, H. Oliva, R. Pacheco, F.O. Faunes, A.E. De Ioannes, M.I. Becker, Hemocyanin of the molluscan *Concholepas concholepas* exhibits an unusual heterodecameric array of subunits, J. Biol. Chem. 279 (2004) 26134–26142.
[15] P. Dolashka-Angelova, M. Schick, S. Stoeva, W. Voelter, Isolation and partial characterization of the N-terminal functional unit of subunit RtH_1 from *Rapana thomasiana* grosse hemocyanin, Int. J. Biochem. Cell Biol. 32 (2000) 529–538.
[16] P. Dolashka-Angelova, St. Stefanovic, A. Dolashki, B. Devreese, B. Tzvetkova, W. Voelter, J. Van Beeumen, B. Salvato, A challenging insight on the structural unit 1 of molluscan *Rapana venosa* hemocyanin, Arch. Biochem. Biophys. 459 (2007) 50–58.
[17] P. Dolashka-Angelova, R. Hristova, S. Stoeva, W. Voelter, Spectroscopic properties of *Carcinus aestuarii* hemocyanin and its structural subunits, Spectrochim. Acta Part A 55 (1999) 2927–2934.
[18] F. Spinozzi, S. Gatto, V. De Filippis, F. Carsughi, P. Di Muro, M. Beltramini, Contribution of the copper ions in the dinuclear active site to the stability of *Carcinus aestuarii* hemocyanin, Arch. Biochem. Biophys. 439 (1) (2005) 42–52.
[19] P. Dolashka-Angelova, A. Dolashki, S. Stevanovic, R. Hristova, B. Atanasov, P. Nikolov, W. Voelter, Structure and stability of arthropodan hemocyanin *Limulus polyphemus*, Spectrochim. Acta Part A 61 (6) (2005) 1207–1217.
[20] B. Tang, Y. Wang, D. Zhang, H. Zhang, Fluorescence properties and conformational stability of the hemocyanin from Chinese mitten crab *Eriocheir japonica sinensis* (Decapoda, Grapsidae), J. Mol. Struct. 920 (1) (2009) 454–458.
[21] R. Toshkova, L. Velkova, W. Voelter, P. Dolashka-Angelova, Protective effect of *Rapana venosa* hemocyanin (RvH) on survivability of hamsters with transplanted myeloid Graffi tumours, C. R. Acad. Bulg. Sci. 59 (9) (2007) 977–982.
[22] I. Iliev, R. Toshkova, P. Dolashka-Angelova, L. Yossifova, R. Hristova, J. Yaneva, S. Zacharieva, Haemocyanins from *Rapana venosa* and *Helix vulgaris* display an antitumour activity via specific activation of spleen lymphocytes, C. R. Acad. Bulg. Sci. 61 (2) (2008) 203–210.
[23] P. Dolashka-Angelova, T. Stefanova, E. Livaniou, L. Velkova, P. Klimentzou, S. Stevanovic, H. Neychev, H. Schwarz, W. Voelter, Immunological potential of *Helix vulgaris* and *Rapana venosa* hemocyanins, Immunol. Investig. 37 (8) (2008) 822–840.
[24] L. Yossifova, I. Iliev, S. Petkova, P. Dolashka-Angelova, L. Mihov, S. Zacharieva, Immunological research on the protective properties of a conjugate of total larval antigen with hemocyanin derived from *Helix vulgaris* against infection with *Trichinella spiralis*, Biotechnol. Biotechnol. Equip. 23 (2) (2009) 597–600.
[25] U. Meissner, C. Gatsogiannis, A. Moeller, F. Depoix, J.R. Harris, J. Markl, Comparative 11 Å structure of two molluscan hemocyanins from 3D cryo-electron microscopy, Micron 38 (2007) 754–765.
[26] P. Dolashka, N. Genov, K. Parvanova, W. Voelter, M. Geiger, S. Stoeva, *Rapana thomasiana* grosse (gastropoda) haemocyanin: spectroscopic studies of the structure in solution and the conformational stability of the native protein and its structural subunits, Biochem. J. 315 (1996) 139–144.
[27] J. Schütz, P. Dolashka-Angelova, R. Abrashev, P. Nikolov, W. Voelter, Isolation and spectroscopic characterization of the structural subunits of keyhole limpet hemocyanin, Biochim. Biophys. Acta 1546 (2001) 325–336.
[28] B.T. Yesilyurt, C. Gielens, F. Meersman, Thermal stability of homologous functional units of *Helix pomatia* hemocyanin does not correlate with carbohydrate content, FEBS J. 275 (14) (2008) 3625–3632.
[29] A. Dolashki, J. Schütz, R. Hristova, W. Voelter, P. Dolashka, Spectroscopic properties of non-glycosilated functional unit KLH 2-c of keyhole limpet hemocyanin, W. J. Agric. Sci. 1 (2) (2005) 129–136.
[30] A. Dolashki, L. Velkova, B. Atanasov, W. Voelter, S. Stevanovic, H. Schwarz, P. Di Muro, P. Dolashka-Angelova, Reversibility and "pH–*T* phase diagrams" of *Rapana venosa* hemocyanin and its structural subunits, Biochim. Biophys. Acta 1784 (2008) 1617–1624.
[31] K. Idakieva, K. Parvanova, S. Todinova, Different scanning calorimetry of irreversible denaturation of *Rapana thomasiana* (marine snail, Gastropod) hemocyanin, Biochem. Biophys. Acta 1748 (2005) 50–56.
[32] L. Bubacco, R.S. Magliozzo, M. Beltramini, B. Salvato, J. Peisach, Preparation and spectroscopic characterization of a coupled binuclear center in cobalt(II)-substituted hemocyanin, Biochemistry 31 (1992) 9294–9303.
[33] Y. Liu, J.M. Sturtevant, The observed change in heat capacity accompanying the thermal unfolding of proteins depends on the composition of the solution and on the method employed to change the temperature of unfolding, Biochemistry 35 (1996) 3059–3062.
[34] P.L. Privalov, N.N. Khechinashvili, B.P. Atanasov, Thermodynamic analysis of thermal transitions of globular proteins. Calorimetric study of chymotrypsinogen, ribonuclease and myoglobin, Biopolymers 10 (1971) 1865–1890.
[35] P.L. Privalov, S.J. Gill, Stability of protein structure and hydrophobic interaction, Adv. Protein Chem. 39 (1988) 191–234.